

GENERALIZED MODELING OF MILLING MECHANICS AND DYNAMICS: PART I - HELICAL END MILLS

Serafettin Engin
Graduate Student
<engin@mech.ubc.ca>

Yusuf Altintas
Professor and ASME Fellow
<altintas@mech.ubc.ca>

The University of British Columbia
Department of Mechanical Engineering
2324 Main Mall, Vancouver, B.C. , V6T 1Z4, CANADA
tel: (604) 822 21 82, fax: (604) 822 24 03

ABSTRACT

Variety of helical end mill geometry is used in industry. Helical cylindrical, helical ball, taper helical ball, bull nosed and special purpose end mills are widely used in aerospace, automotive and die machining industry. While the geometry of each cutter may be different, the mechanics and dynamics of the milling process at each cutting edge point are common. This paper presents a generalized mathematical model of most helical end mills used in industry. The end mill geometry is modeled by helical flutes wrapped around a parametric envelope. The coordinates of a cutting edge point along the parametric helical flute are mathematically expressed. The chip thickness at each cutting point is evaluated by using the true kinematics of milling including the structural vibrations of both cutter and workpiece. By integrating the process along each cutting edge, which is in contact with the workpiece, the cutting forces, vibrations, dimensional surface finish and chatter stability lobes for an arbitrary end mill can be predicted. The predicted and measured cutting forces, surface roughness and stability lobes for ball, helical tapered ball, and bull nosed end mills are provided to illustrate the viability of the proposed generalized end mill analysis.

NOMENCLATURE:

P : A cutting point on cutting edge
X, Y, Z : Global stationary coordinate sys. as shown in Figure 3
a : Axial depth of cut
dz : Differential height of the chip segment
h : Valid cutting edge height from tool tip
h(ψ, φ, z) : Chip thickness at a cutting point specified by $(ψ, φ, z)$
i(z) : Helix angle
lead : Lead value for constant lead
n : Spindle speed
r(z) : Radial coordinate of a cutting edge point
α, β : Parametric angles of the end mill
φ : Rotation angle of cutting edge
ψ(z) : Cutting edge position angle at level *z* on the XY plane

F_x, F_y, F_z : Force components in X, Y and Z directions
D, R, R_r, R_z : Parametric radial dimensions of the end mill
M_r, N_r : Radial offsets of the end mill profile for points *M* and *N*
M_z, N_z : Axial offsets of the end mill profile for points *M* and *N*
N_f : Number of flutes
K_{te}, K_{rc}, K_{ac} : Cutting force coefficients in tangential, radial and axial directions
K_{te}, K_{re}, K_{ae} : Edge force coefficients in tangential, radial and axial directions
dF_r, dF_t, dF_a : Differential tangential, radial and axial forces
r̄(z) : Vector from tool center to cutting edge
s_{ij} : Feed per tooth for tooth *j* $\left(s_{ij} = \frac{\text{feedrate} \cdot \phi_{pj}}{n \cdot 2\pi} \right)$
x_j, y_j, z_j : Coordinates of point ***P*** which is in cutting
φ_j(z) : Total angular rotation of flute *j* at level *z* on the XY pl.
φ_{pj} : Pitch angle of flute *j*
[*T*] : Transformation matrix for the cutting forces

1. INTRODUCTION

Variety of helical end mill geometry is used in milling operations. Simple cylindrical helical end mills are used in peripheral milling of prismatic parts. Straight and helical ball end mills are widely used in machining sculptured die and aerospace part surfaces, and bull nosed cutters produce periphery of parts meeting with the bottom floor with fillets. Tapered helical end mills are used in five axis machining of jet engine compressors, and form cutters are used to open complex profiles such as turbine blade carrier rings. A classical approach in the literature has been to develop milling mechanics models for each cutter shape, therefore, mechanics and dynamics models developed individually for face (Fu *et al.*, 1984), cylindrical (Sutherland *et al.* 1986, Bayoumi *et al.* 1994; Budak *et al.*, 1996; Spiewak, 1994), ball end (Lazoglu *et al.*, 1997; Altintas *et al.*, 1998; Yucesan *et al.*, 1996) and tapered ball end mills (Ramaraj *et al.*, 1994) have been reported in the literature. Ehmman *et al.* (1997) summarized the overview of past research in mechanics and dynamics of milling, which were mainly specific to standard end and face milling cutters. A generalized

mechanics and dynamics model that can be used to analyze any cutter geometry is therefore required in order to analyze variety of end mill shapes used in manufacturing industry.

The cutter geometry has two geometric components. The envelope or outer geometry of the cutter is used in generating NC tool paths on CAD/CAM systems. Moreover, the envelope of the cutter is used in identifying the intersection of cutter and workpiece geometry, which is required in simulating the material removal process and in dynamically updating the blank geometry for graphical NC tool path verification (Leu *et al.*, 1997; Gu *et al.*, 1997; Spence *et al.*, 1994). The geometric model must also include the cutting edge geometry along the flutes for analyzing the mechanics and dynamics of the milling process. The prediction of the cutting forces and vibrations require the coordinates, as well as rake, helix, clearance angles of the cutting edge point on the flute (Budak *et al.*, 1996).

A generalized model of end mill geometry and cutting flutes is introduced in this paper. The envelope of the geometry is defined similar to the parametric representation used by APT (Childs, 1973) and CAD/CAM software systems. The formulation of cutting edge coordinates is presented. It is shown that a vast variety of helical end mill geometry can be designed using the proposed geometric model of generalized cutters. The modeled cutting edge can be broken into small increments, where the cutting constant may be different at each location. As an example, helical ball, tapered helical ball and bull nose cutters are provided. It is experimentally proven that the model can be used in predicting the cutting forces, vibrations, dimensional surface finish, as well as chatter stability lobes for any cutter geometry.

2. GENERALIZED GEOMETRIC MODEL OF MILLING CUTTERS

APT and CAD/CAM systems define the envelope of milling cutters by seven geometric parameters (Childs, 1973):

$$\text{CUTTER/ } D, R, R_r, R_z, \alpha, \beta, h$$

where the cutter parameters D , R , R_r , R_z , α , β and h are shown in Figure 1. The generalized parametric statement can define a variety of face and helical end mill shapes used in industry as shown in Figure 2. These seven geometric parameters are independent of each other, but with geometric constrains in order to create mathematically realizable shapes. A helical cutting edge is wrapped around the end mill envelope as shown in Figure 3. The mechanics of cutting require the identification of coordinates, the local cutting edge geometry, chip load, and the three differential cutting forces (dF_a , dF_r , dF_t) at cutting points (i.e. P in Figure 3) along the cutting edge. Point P has elevation z , radial distance $r(z)$ on XY plane, axial immersion angle $\kappa(z)$ and radial lag angle $\psi(z)$. The axial immersion angle is defined as the angle between the cutter axis and normal of helical cutting edge at point P (Figure 3). The radial lag angle is the angle between the line, which connects the point P to the cutter tip on the XY plane and the cutting edge tangent at the tip of the cutter. The coordinates of P are defined by vector $\vec{r}(z)$ in cylindrical coordinates.

The periphery of the milling cutter is divided into three zones (Figure 1):

$$\left. \begin{aligned} r(z) &= \frac{z}{\tan \alpha} && \text{for zone } OM \\ r(z) &= \sqrt{R^2 - (R_z - z)^2} + R_r && \text{for zone } MN \\ r(z) &= u + z \tan \beta, \quad u = \frac{D}{2}(1 - \tan \alpha \tan \beta) && \text{for zone } NS \end{aligned} \right\} (1)$$

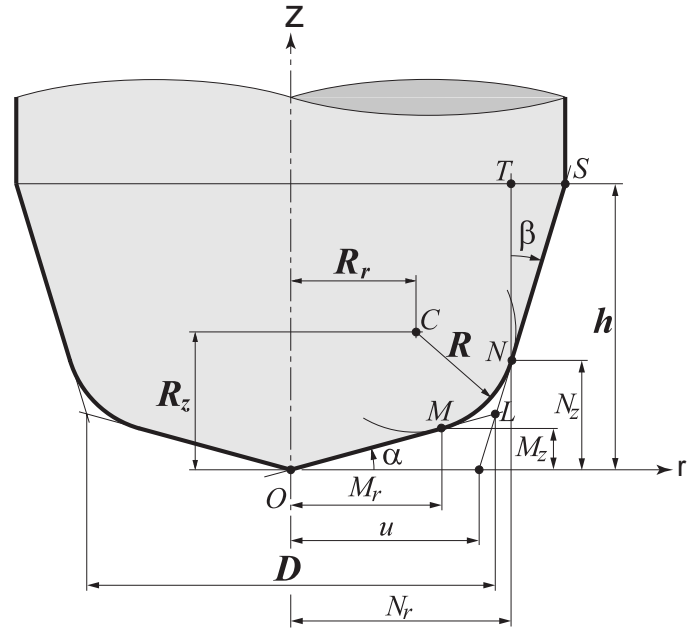


Figure 1. General tool geometry.

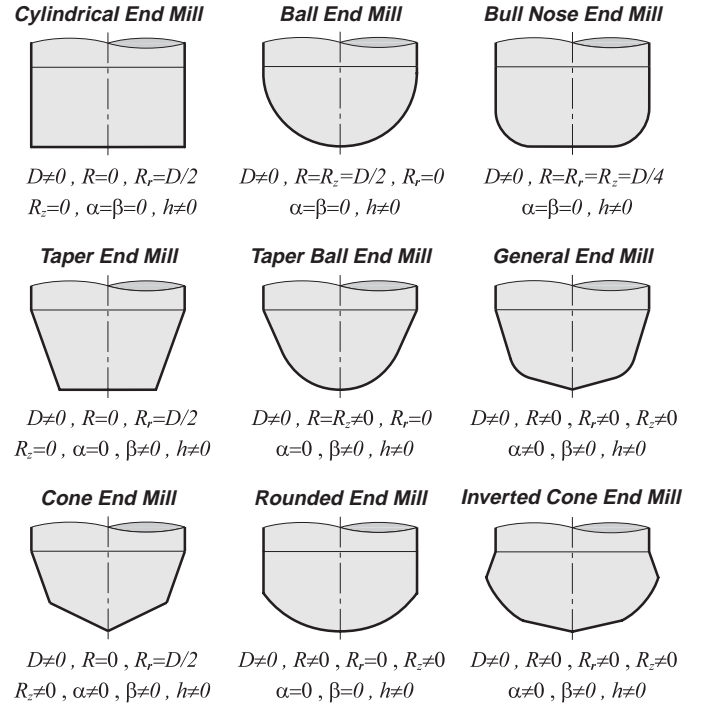


Figure 2. End mill shapes.

where $r(z)$ is the radius of the cutter at elevation z , u is the distance between the cutter tip and the point at which the NS line intersects the XY plane.

An arc with the center at point C , a radial offset R_r and arc radius of R , is tangent to or intersects the taper lines OL and LS at points M and N , respectively (Figure 1). The radial and axial offsets of points M and N from the cutter axis and tip are found, respectively, as:

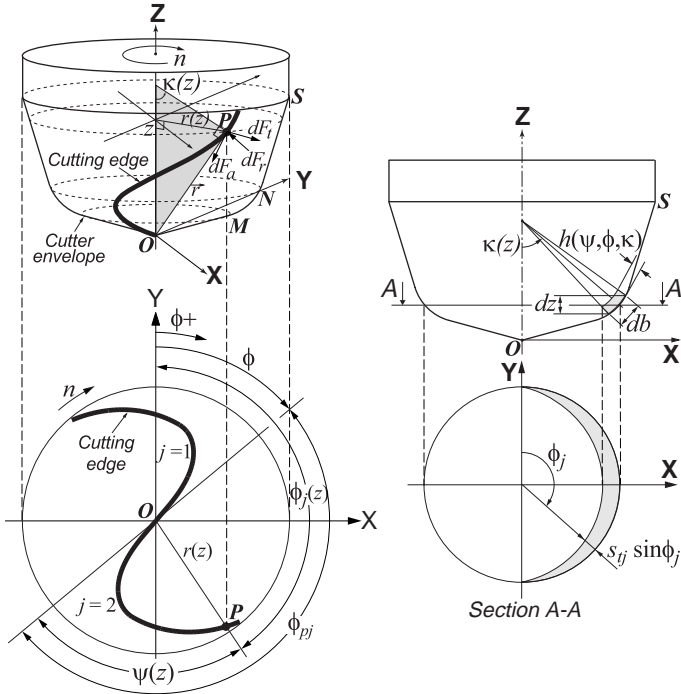


Figure 3. Geometric model of the general end mill.

$$\left. \begin{aligned} M_r &= \frac{R_z \tan \alpha + R_r + \sqrt{(R^2 - R_r^2) \tan^2 \alpha + 2R_z R_r \tan \alpha - R_z^2 + R^2}}{\tan^2 \alpha + 1} \\ M_z &= M_r \tan \alpha \quad \text{for } 0 \leq \alpha < 90 \end{aligned} \right\} (2)$$

and

$$\left. \begin{aligned} N_r &= \frac{(R_r - u) \tan \beta + R_z - \sqrt{(R^2 - R_z^2) \tan^2 \beta + 2R_z (R_r - u) \tan \beta - (R_r - u)^2 + R^2}}{\tan^2 \beta + 1} \\ N_z &= u + N_r \tan \beta \quad \text{for } \beta < 90 \end{aligned} \right\} (3)$$

In Figure 1, the lines **OM** and **SN** are not necessarily tangent to the corner arc at the points **M** and **N**. If the lines are tangent to the arc, outer surface of the cutter will be continuous through out the three segments, otherwise the surface will be discontinuous so as the helix angle.

The radial offset at elevation z and the axial immersion angle in three zones are (Figure 1, Figure 3),

$$\left. \begin{aligned} &\text{for along line } \mathbf{OM}: \\ &\quad r(z) = \frac{z(\psi)}{\tan \alpha}, \quad \kappa(z) = \alpha \\ &\text{for along arc } \mathbf{MN}: \\ &\quad r(z) = R_r + \sqrt{R^2 - (R_z - z(\psi))^2}, \quad \kappa(z) = \sin^{-1} \left(\frac{r(z) - R_r}{R} \right) \\ &\text{for along line } \mathbf{NS}: \\ &\quad r(z) = N_r + (z(\psi) - N_z) \tan \beta, \quad \kappa(z) = \frac{\pi}{2} - \beta \end{aligned} \right\} (4)$$

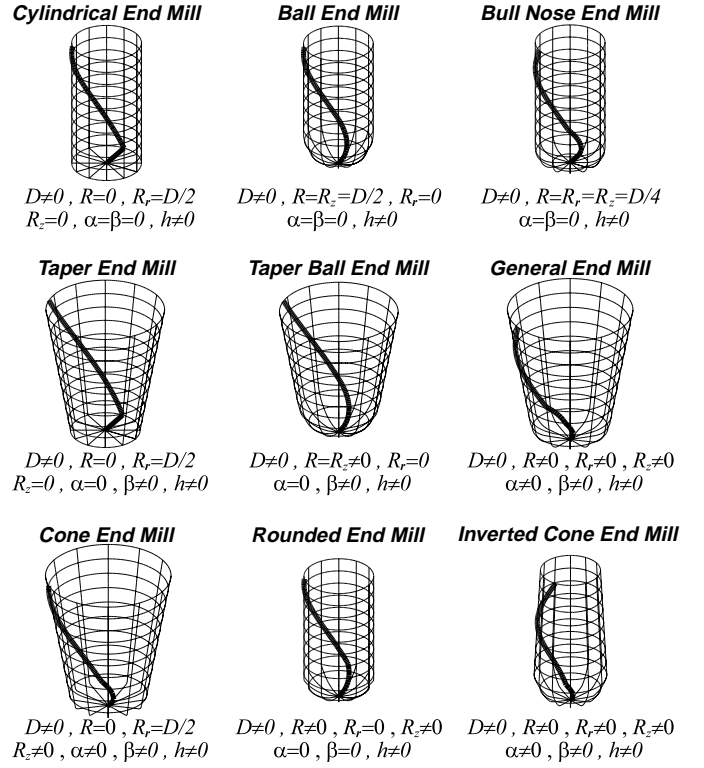


Figure 4. Helical cutting edges on the tool.

2.1 Generalized Geometric Model of the Helical Cutting Edges

Helical flutes can be wrapped around the cutters as shown in Figure 4. A vector drawn from cutter tip (**O**) to any point (**P**) on a helical flute can be expressed as (Figure 3),

$$\vec{r}_j = x_j \vec{i} + y_j \vec{j} + z_j \vec{k} = r(\phi_j) (\sin \phi_j \vec{i} + \cos \phi_j \vec{j}) + z(\phi_j) \vec{k} \quad (5)$$

where ϕ_j is the radial immersion angle of point **P** on flute number j . The radial immersion angle (ϕ_j) varies as a function of rotation angle, flute position, and the local helix angle at point **P**. The first flute ($j=1$) is considered to be a reference edge, and its rotation angle at the elevation $z=0$ is ϕ . The immersion angle for flute j at axial location z is expressed as:

$$\phi_j(z) = \phi + \sum_{n=1}^j \phi_{pj} - \psi(z) \quad (6)$$

where ϕ_{pj} is the pitch angle between the preceding flutes. It should be noted that this general formulation allows variable pitch cutters as well. The radial lag angle $\psi(z)$ due to the local helix angle i . Since the cutter diameter may be different along the axis, the helix and thus lag angles vary along the flute as well, and they are evaluated in the following subsection.

An infinitesimal length (dS) of a helical cutting edge segment can be given as follows,

$$\left. \begin{aligned} dS &= |dr| = \sqrt{r^2(\phi) + (r'(\phi))^2 + (z'(\phi))^2} d\phi \\ r'(\phi) &= \frac{dr(\phi)}{d\phi}, \quad z'(\phi) = \frac{dz(\phi)}{d\phi} \end{aligned} \right\} (7)$$

The chip thickness changes with both radial (ϕ_j) and axial immersion (κ) as the following,

$$h(\phi_j) = s_{ij} \sin \phi_j \sin \kappa \quad (8)$$

where s_{ij} is the feed per tooth for tooth j . Note that the effective feed for every tooth may be different when variable pitch cutters are used. The lag angle $\psi(z)$ has a different expression for each zone along the flute, which is wrapped around general cutter geometry.

Zone OM ($z \leq M_z$): The helix angle is assumed to be constant at this usually small cone part, i.e. $i(z) = i_o$. Ramaraj (1994) gives the differential equation and its solution for a helical flute spiraled on a cone as,

$$\frac{dr}{d\psi} - \frac{\cos \alpha}{\tan i_o} r = 0 \quad \text{and therefore} \quad r = e^{(\cos \alpha / \tan i_o) \psi} \quad (9)$$

Since the spiral radius is zero at the tool tip, the lag angle condition becomes $\psi(0) = -\infty$. Instead, the simulations were started with a small radial offset from the tip, i.e. $r_s = M_r / 20$ which gives a starting lag angle of $\psi_{1s} = \ln r_s \tan i_o / \cos \alpha$. The variation of lag angle along the helical flute is evaluated from Eq. (9),

$$\psi(z) = \frac{\ln(z \cot \alpha) \tan i_o}{\cos \alpha} - \psi_{1s} \quad (10)$$

The final lag angle at the point M becomes $\psi_{1e} = \frac{\ln M_r \tan i_o}{\cos \alpha} - \psi_{1s}$.

If the cone zone (**OM**) does not exist (i.e. bull nose and ball end cutters), α , ψ_{1s} and ψ_{1e} will be zero.

Arc Zone MN ($M_z < z \leq N_z$): Due to changing radial offset from the cutter axis, the helix angle varies along the flute for constant lead cutters as,

$$i(z) = \tan^{-1} \left[\frac{(r(z) - R_r) \tan i_o}{R} \right] \quad (11)$$

Since the arc is not a full quarter due to tangency to the cone, there is a discontinuity on the helix angle at point M . This leads to the following lag angle expression,

$$\psi(z) = \frac{(R + z - R_z) \tan i_o}{R} - \psi_{as} + \psi_{1e} \quad (12)$$

where ψ_{1e} and ψ_{as} are the final lag angles at point M formed by the cone and arc, respectively. The lag angle (ψ_{as}) formed by the arc at point M is,

$$\psi_{as} = \frac{(R + M_z - R_z) \tan i_o}{R} \quad (13)$$

The final lag angle at the end point N of the arc is:

$$\psi_{ae} = \frac{(R + N_z - R_z) \tan i_o}{R} - \psi_{as} + \psi_{1e} \quad (14)$$

if the arc is missing from the cutter geometry $R = 0 \rightarrow \psi_{as} = 0$, $\psi_{ae} = \psi_{1e}$.

Taper Zone NS ($N_z < z$): The taper zone of the cutters is ground either with a constant lead or constant helix. The constant lead, which leads to variable helix angle along the flute, is preferred by the cutter grinders in order to save from the material during re-grinding operation. However, cutting mechanics are more uniform with constant helix cutters, which require varying lead. Both methods are modeled here.

Constant helix: The helix angle is constant, and the lag angle changes along the flute:

$$\left. \begin{aligned} i(z) &= i_o \\ \psi(z) &= \frac{\ln(N_r - (N_z - z) \tan \beta) \tan i_o}{\sin \beta} - \psi_{2s} + \psi_{ae} \quad \text{if } \beta \neq 0 \\ \psi(z) &= \frac{(z - N_z) \tan i_o}{N_r} - \psi_{2s} + \psi_{ae} \quad \text{if } \beta = 0 \end{aligned} \right\} \quad (15)$$

where ψ_{ae} and ψ_{2s} are final lag angle at the point N from the arc and initial lag angle generated by the taper zone (**NS**) at point N , respectively. The initial value ψ_{2s} is,

$$\left. \begin{aligned} \psi_{2s} &= \frac{\ln(N_r) \tan i_o}{\sin \beta} \quad \text{if } \beta \neq 0 \\ \psi_{2s} &= 0 \quad \text{if } \beta = 0 \end{aligned} \right\} \quad (16)$$

The final value ψ_{2e} at point S is,

$$\left. \begin{aligned} \psi_{2e} &= \frac{\ln(N_r - (N_z - h) \tan \beta) \tan i_o}{\sin \beta} - \psi_{2s} + \psi_{ae} \quad \text{if } \beta \neq 0 \\ \psi_{2e} &= \frac{(h - N_z) \tan i_o}{N_r} + \psi_{ae} \quad \text{if } \beta = 0 \end{aligned} \right\} \quad (17)$$

Constant Lead: The lead of the helical flute is constant, and the helix varies along the flute. The nominal helix (i_s) and lead (*lead*) of the of the tapered flute is defined at point N ,

$$i_s = \tan^{-1} \left[\frac{2\pi N_r}{\text{lead} \cdot \cos \beta} \right] \quad (18)$$

which leads to a variable helix expression

$$i(z) = \tan^{-1} \left[\frac{(\psi - \psi_{ae}) r(z)}{z - N_z} \right] \quad (19)$$

The variation of the lag angle $\psi(z)$ is given by,

$$\psi(z) = \frac{(z - N_z) \tan i_s}{N_r} + \psi_{ae} \quad \text{for } N_z \leq z \leq h \quad (20)$$

3. MODELING OF CUTTING FORCES

The differential tangential (dF_t), radial (dF_r) and axial (dF_a) cutting forces acting on infinitesimal cutting edge segment are given by (Altintas and Lee, 1998),

$$\left. \begin{aligned} dF_t &= K_{te} dS + K_{tc} h(\phi, \kappa) db \\ dF_r &= K_{re} dS + K_{rc} h(\phi, \kappa) db \\ dF_a &= K_{ae} dS + K_{ac} h(\phi, \kappa) db \end{aligned} \right\} \quad (21)$$

where $h(\phi, \kappa)$ is the uncut chip thickness normal to the cutting edge and varies with the position of the cutting point and cutter rotation. Subindices (c) and (e) represent shear and edge force components, respectively. The edge cutting coefficients K_{te} , K_{re} and K_{ae} are constants and related to the cutting edge length dS given in Eq (7). The shear force coefficients K_{tc} , K_{rc} , K_{ac} are identified either mechanistically from milling tests conducted at a range of feed rate (Fu *et al.*, 1984; Yucesan and Altintas 1996) or a set of orthogonal cutting tests using an oblique transformation method presented by Budak *et al.* (1996). db ($db = dz/\sin \kappa$) is the projected length of an infinitesimal cutting flute in direction along the cutting velocity. The chip thickness $h(\phi, \kappa)$ is evaluated using the true kinematics of milling (Martellotti, 1945) as well as the vibration of both the cutter and workpiece. The cutter is rotated at a spindle speed and the workpiece is fed with the given feed using a small discrete time interval. The positions of cutting points along the flute are evaluated using the geometric model presented in section 2. The location of the same flute point on the cut surface is identified using both the rigid body kinematics as well as structural displacements of cutter and workpiece. The dynamic chip thickness is evaluated by subtracting the present coordinate of the cutting point from the previous surface generated by the preceding tooth. The mathematical model and the procedure to evaluate dynamic chip load are well explained for the helical cylindrical and ball end mills in the previous publications (Montgomery and Altintas, 1991; Altintas and Lee, 1998), and not repeated here due to similarity of the approaches. Once the chip load is identified and cutting constants are evaluated for the local edge geometry, the cutting forces in Cartesian coordinate system can be evaluated as,

$$\{dF_{xyz}\} = [T] \{dF_{rta}\} \quad (22)$$

or

$$\begin{bmatrix} dF_x \\ dF_y \\ dF_z \end{bmatrix} = \begin{bmatrix} -\sin \phi \sin \kappa & -\cos \phi & -\sin \phi \cos \kappa \\ -\cos \phi \sin \kappa & \sin \phi & -\cos \phi \cos \kappa \\ -\cos \kappa & 0 & -\sin \kappa \end{bmatrix} \begin{bmatrix} dF_r \\ dF_t \\ dF_a \end{bmatrix} \quad (23)$$

The total cutting forces for the rotational position ϕ can be found integrating Eq. (23) along the axial depth of cut for all cutting flutes which are in contact with the workpiece.

$$F_x(\phi) = \sum_{j=1}^{N_f} F_{xj}[\phi(z)]$$

$$F_y(\phi) = \sum_{j=1}^{N_f} F_{yj}[\phi(z)]$$

$$F_z(\phi) = \sum_{j=1}^{N_f} F_{zj}[\phi(z)]$$

$$\left. \begin{aligned} F_x &= \sum_{j=1}^{N_f} \int_{z_1}^{z_2} \begin{bmatrix} -dF_{rj} \sin \phi_j \sin \kappa_j & -dF_{tj} \cos \phi_j & -dF_{aj} \sin \phi_j \cos \kappa_j \end{bmatrix} dz \\ F_y &= \sum_{j=1}^{N_f} \int_{z_1}^{z_2} \begin{bmatrix} -dF_{rj} \cos \phi_j \sin \kappa_j & dF_{tj} \sin \phi_j & -dF_{aj} \cos \phi_j \cos \kappa_j \end{bmatrix} dz \\ F_z &= \sum_{j=1}^{N_f} \int_{z_1}^{z_2} \begin{bmatrix} -dF_{rj} \cos \phi_j & & -dF_{aj} \sin \kappa_j \end{bmatrix} dz \end{aligned} \right\} \quad (24)$$

where N_f is the number of flutes on the cutter. z_1 and z_2 are the contact boundaries of the flute within the cut and can be found from the geometric model of each zone given in section 2. The cutter is

axially digitized with small disk elements with a uniform differential height of dz . The differential cutting forces are calculated along the full contact length for all flutes which are in cut, and digitally summed to find the total cutting forces $F_x(\phi)$, $F_y(\phi)$ and $F_z(\phi)$ at a given rotation angle $\phi = \Omega \cdot dt$ where Ω (rad/s) is the spindle speed and dt is the differential time interval for digital integration.

The structural dynamics of both cutter and workpiece are measured at the tool tip, and the modes are identified using experimental modal analysis technique. The dynamic chip thickness, cutting forces, vibrations, surface finish, torque and moments generated by the interaction of cutting forces and structural dynamics are simulated in the time domain using a technique similar to one presented for ball end milling by Altintas and Lee (1998). The chatter stability lobes are predicted both using time domain simulations and frequency domain analytical chatter stability prediction method presented previously by Altintas *et al.* (1995, 1998, 1999). The readers are referred to the previous literature for the mathematical details of the time and frequency domain solutions of the dynamic milling process.

4. SIMULATION AND EXPERIMENTAL RESULTS

More than 300 cutting tests with various cutter geometry and material were conducted using the generalized method presented here. A sample of helical and inserted end mills are presented here to demonstrate the flexibility of the proposed model.

Tapered Helical Ball End Mill: These cutters are mainly used in five axis milling of jet engine compressors made of Titanium Ti_6Al_4V alloys. Because of large axial depth of cuts and poor machinability of Titanium, the chip loads are small and the cutting speed is low in order to avoid shank breakage and edge chipping. Chatter vibrations are also most frequently experienced due to heavy cuts with slender end mills. The proposed model is applied to the design and virtual analysis of the tapered cutters for an aircraft jet engine company. The objective was to optimize the cutting tool geometry for strength, and identify the chatter stability lobes to avoid self-excited vibrations during milling compressors and integral bladed rotors. The cutting constants for Ti_6Al_4V are identified using orthogonal to oblique cutting transformation method and given in (Budak *et al.*, 1996). One of the particular cutter geometry generated by the proposed geometric model is given in Figure 5. Although the tests were conducted at various depth of cuts and feeds, two sample predictions and experimental validations are given in Figure 6. The tests cover both the ball end and tapered zones. The higher axial depth of cuts produced severe chatter vibrations on our machining center, which does not have a spindle as rigid as the five axis machining centers used in our industrial partner's shop. Even though the orthogonal cutting database is used, the predicted and measured cutting forces are in satisfactory agreement.

Ball End Cutters: Ball end mills are used mostly in die and mold machining industry. The surface finish, static form errors, chatter vibrations, and tool life are the main constrains in ball end milling of dies and molds. The prediction of ball end milling forces and cutting constants (Yucesan and Altintas, 1996), chatter stability (Altintas *et al.*, 1999), and surface finish (Altintas and Lee, 1998) were presented before using specific geometric model of ball end mills. Slot ball end milling tests and predicted cutting forces are shown in Figure 7. The cutter material was WC coated with TiAlON, the work material was GGG70 spheroidal graphite cast iron with 251-283HB hardness, and the cutting conditions are given in Figure 7.

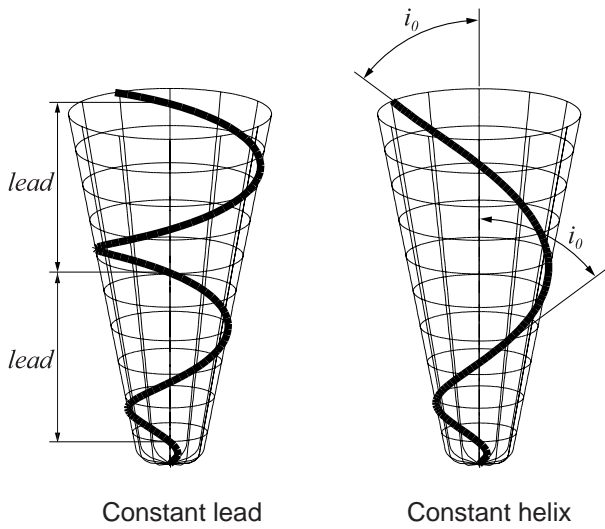


Figure 5. Taper helical ball end mill. Constant lead and constant helix on the taper.

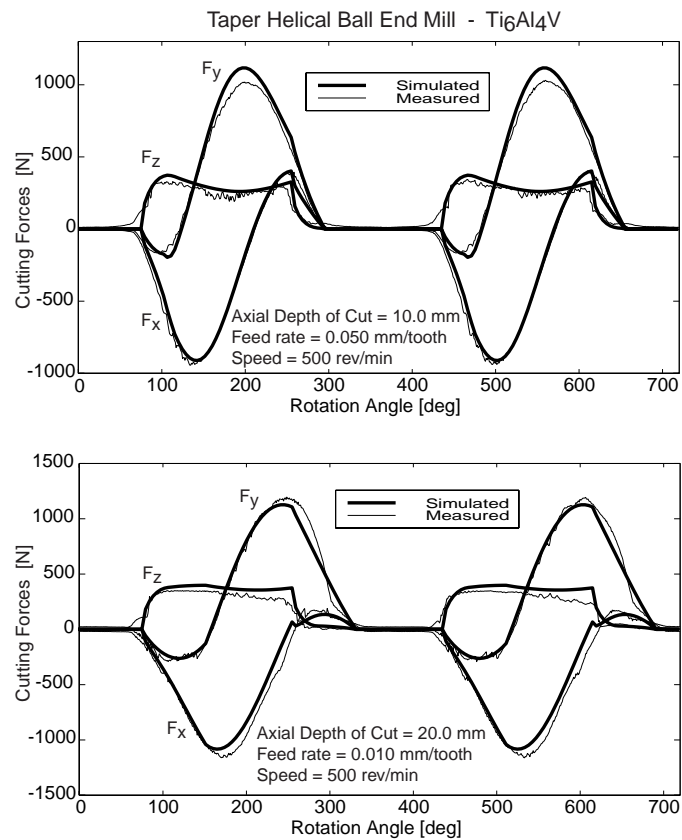


Figure 6. Measured and predicted cutting forces for slot cutting. Cutting conditions: rake angle = 10° , relief angle = 10° , tool type is taper helical ball end mill, $D = 6.0$ mm, $R = 3.0$ mm, $R_r = 0$ mm, $R_z = 3.0$ mm, $\alpha = 0^\circ$, $\beta = 4.0^\circ$, $h = 38.0$ mm, $lead = 105.0$ mm, $N_f = 1$ flute, carbide cutter, see reference (Budak *et al.*, 1996) for Ti_6Al_4V orthogonal cutting coefficients.

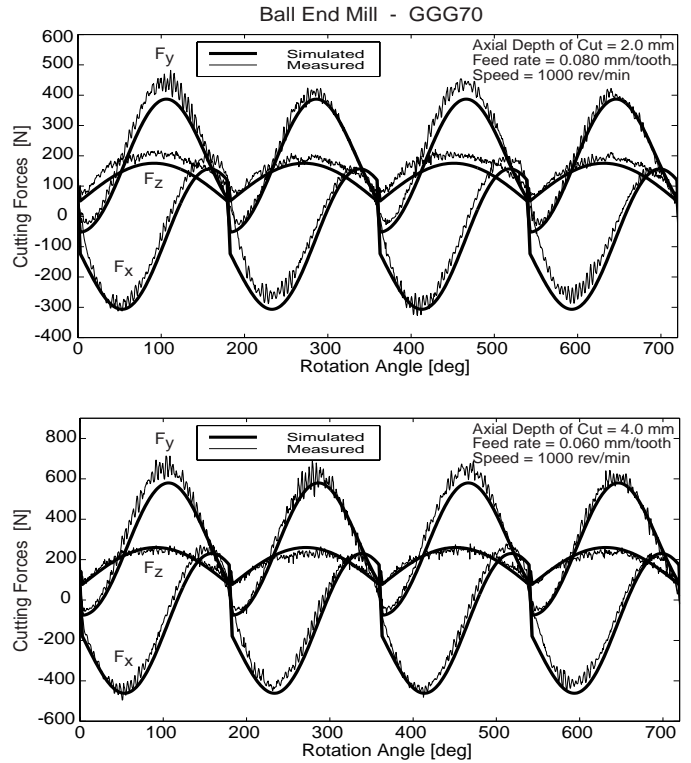
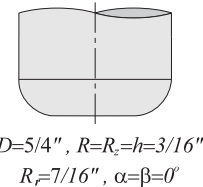


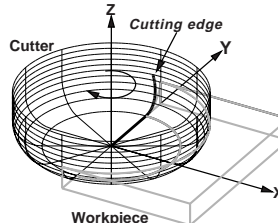
Figure 7. Measured and predicted cutting forces for slot cutting. Cutting conditions: rake angle = 10° , relief angle = 0° , tool type is ball end mill, $D = 12.0$ mm, $R = R_r = 6.0$ mm, $R_z = 0$ mm, $\alpha = 0^\circ$, $\beta = 0^\circ$, $h = 6.0$ mm, $N_f = 2$ flutes, cutter material was WC coated with TiAlON, workpiece material GGG70 spheroidal graphite, Cutting coefficients: $K_{tc}=2172.1$, $K_{rc}=848.90$, $K_{ac}=-725.07$ N/mm², $K_{te}=17.29$, $K_{re}=7.79$, $K_{ae}=-6.63$ N/mm.

CUTTER MODEL

Bull Nose End Mill



3D CUTTER MODEL

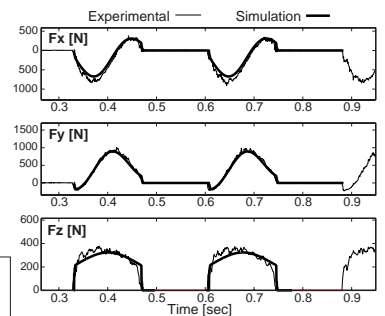


Cutting Conditions:
 Spindle speed (n) = 217 rev/min
 Axial Depth of Cut (a) = 4.0 mm, Ti_6Al_4V
 Feed Rate (s_f) = 0.100 mm/tooth, slotting
 Only one insert is used during the cutting test.

REAL CUTTER



CUTTING FORCES



NOTE: Cutting Coefficients are obtained from Orthogonal Cutting Experiments.

Figure 8. General tool geometry application for inserted end mill. See reference (Budak *et al.*, 1996) for the cutting coefficients.

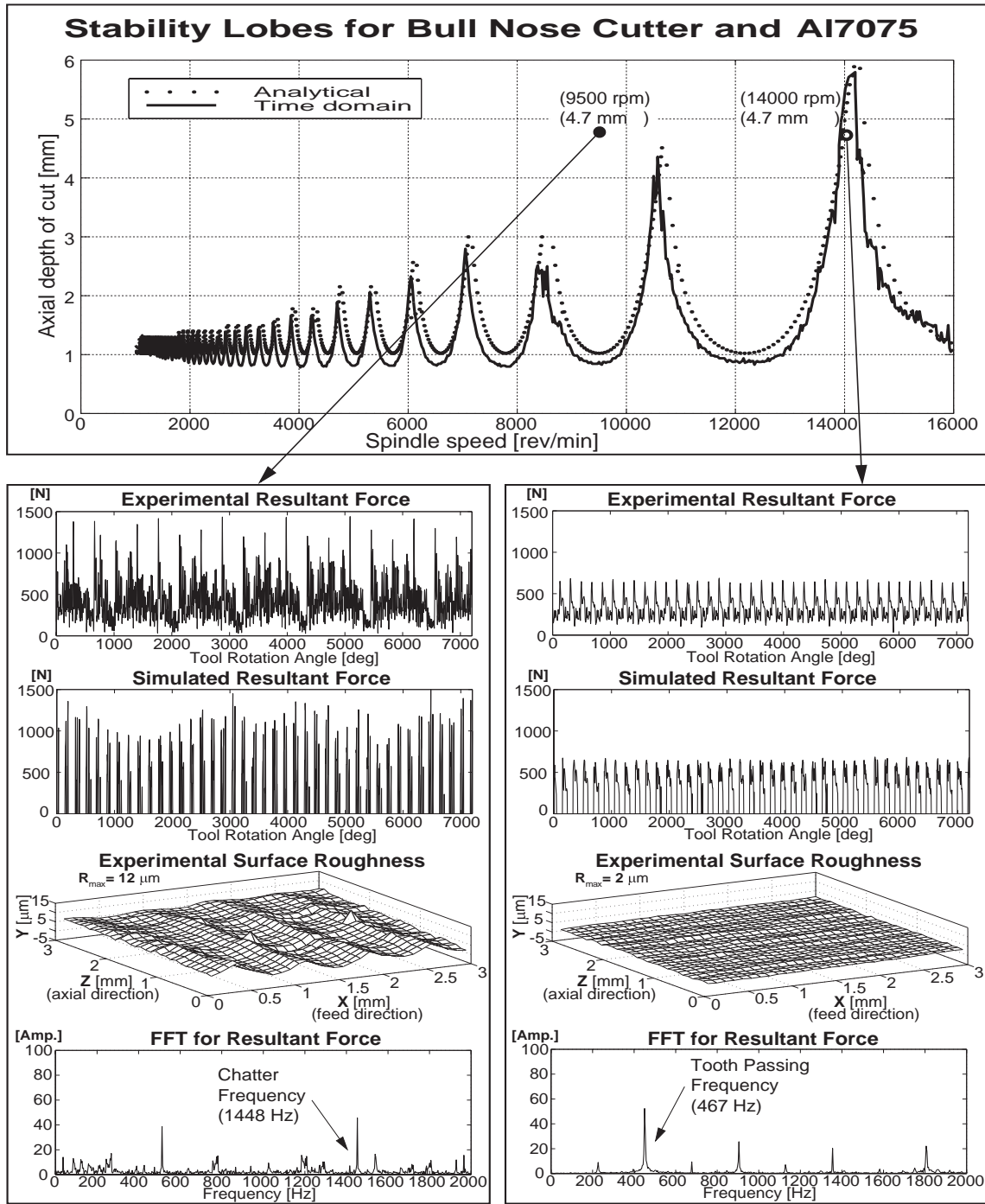


Figure 9. Stability lobes for Bull nose cutter (see Figure 8). Cutting conditions: half immersion down milling, $N_f = 2$ flutes, feed rate 0.050 mm/tooth. See Table 1 for the transfer function parameters. Average cutting coefficients for Al-7075: $K_{tc}=1319.41$, $K_{rc}=788.83$, $K_{ac}=48.75$ N/mm², $K_{te}=19.65$, $K_{re}=26.77$, $K_{ae}=2.05$ N/mm.

Bull Nosed Cutter: A bull nosed cutter with two coated circular inserts is used in milling Titanium Ti_6Al_4V and Aluminum Al-7075 alloys. The cutter was first designed using the proposed general geometric model as shown in Figure 8. The cutting forces are predicted for slot milling of Ti_6Al_4V with one insert. The orthogonal

cutting database was used in evaluating the average cutting constants. The simulated and measured cutting forces were found to be in good agreement as shown in Figure 8. The same cutter was also tested on Al-7075. The transfer function of the cutter attached to taper 40 spindle with a mechanical chuck is given in Table 1. The transfer function model has the following structure:

$$\frac{x}{F} = [\Phi_{xx}(s)] = \sum_{k=1}^K \frac{[R_{1x} + R_{2x}s]_k}{s^2 + 2\zeta_{x,k}\omega_{x,k}s + \omega_{x,k}^2}$$

where x, F are the vibration and force in the feed direction, respectively. $\zeta_{x,k}, \omega_{x,k}$ are the damping ratio and natural frequency for mode k , and K is the number modes. The modal parameters are evaluated from estimated complex mode residues ($\sigma_k \pm i\nu_k$) as $R_{1x,k} = 2(\zeta_{x,k}\omega_{nx,k}\sigma_k - \omega_{dx,k}\nu_k)$, $R_{2,k} = 2\sigma_k$. Similar terminology is used in the normal direction (Y). The chatter stability lobes of the system are predicted both in time and frequency domains, see Figure 9. The analytical stability solution is accurate, computationally fast, and agrees well with the stability lobes predicted by time consuming, iterative time domain solutions (Altintas and Budak, 1995). The stability diagram indicates chatter free milling speed at 14000 rev/min with an axial depth of cut 4.7 mm. The same axial depth is predicted to produce significant chatter at the lower spindle speed of 9500 rev/min. The simulated and experimentally measured cutting forces, simulated surface finish, forced and chatter vibration frequencies indicate the correctness of the proposed model. At 14000 rev/min spindle speed, there is no chatter, the cutting forces have regular static pulsation at tooth passing frequency, and the predicted surface finish is smooth. At 9500 rev/min, there is chatter at 1448 Hz which coincides to second bending mode of the spindle in the feed direction, the force magnitudes are at least twice larger than chatter free machining test, and the surface is quite wavy.

Table 1. Measured modal parameters of the bull nose inserted cutter on a machining center.

Direction	Mode	ω_n [Hz]	ζ [%]	Mode Residue [m/N] ($\sigma_k \pm i\nu_k$)
X	1	452.77	12.37	$(92.02966 - i 186.2195) \cdot 10^{-6}$
	2	1448.53	1.65	$(-41.81562 - i 304.362) \cdot 10^{-6}$
Y	1	516.17	2.43	$(-2.39290 - i 172.1539) \cdot 10^{-6}$
	2	1407.64	3.24	$(40.55052 - i 361.8808) \cdot 10^{-6}$

The authors conducted various cutting tests with helical ball and cylindrical helical end mills and obtained similar results. The objective of the research has been to design a virtual milling simulation system which can handle a variety of different end mills for improved cutter design or process planning in industry.

5. CONCLUSION

A generalized mathematical model of arbitrary end mills is presented. The model allows parametric design and representation of variety of end mill shapes and helical flutes. Sample design examples include cylindrical, ball, tapered helical end mills as well as inserted bull nosed cutters. The model allows evaluation of local cutting edge geometry along the flute. Using previously developed exact kinematics of dynamic milling, the chip thickness and the corresponding cutting forces, vibrations, and dimensional surface finish generated by end mills with arbitrary geometry. The mathematical models are supported by a number of experiments conducted with helical tapered end, ball end and bull nosed cutters. The proposed approach allows the design and analysis of variety of milling operations used in industry.

ACKNOWLEDGEMENTS

This research is supported NSERC, General Motors and Boeing under Cooperative Research and Development Research Grant (NSERC 11R80193).

REFERENCES

- Altintas, Y. and Lee, P., 1998, "Mechanics and Dynamics of Ball End Milling", *Transaction of ASME, Journal of Manufacturing Science and Engineering*, Vol. 120, pp. 684-692.
- Altintas, Y., and Budak, E., 1995, "Analytical Prediction of Stability Lobes in Milling", *Annals of CIRP*, Vol. 44(No.1), pp. 357-362.
- Altintas, Y., Shamoto, E., Lee, P., and Budak, E., 1999, "Analytical Prediction of Stability Lobes in Ball End Milling", *Transactions of ASME Journal of Manufacturing Science and Engineering*, (in press).
- Bayoumi A. E., Yucesan, G., and Kendall, L. A., 1994, "An Analytic Mechanistic Cutting Force Model for Milling Operations: A Theory and Methodology", *Transaction of the ASME*, Vol. 116, pp. 324-330.
- Budak, E., Altintas, Y. and Armarego, E.J.A., 1996, "Prediction of Milling Force Coefficients from Orthogonal Cutting Data", *Transactions of ASME*, Vol. 118, pp. 216-224.
- Childs, J. J., 1973, "Numerical Control Part Programming", *Industrial Press*.
- Ehmann, K. F., Kapoor, S. G., DeVor, R. E., and Lazoglu, I., 1997, "Machining Process Modeling: A Review", *Journal of Manufacturing Science and Engineering Transaction of the ASME*, Vol. 119(No.4-B), pp. 655-663.
- Fu, H. J., Devor, R. E., and Kapoor, S. G., 1984, "A Mechanistic Model for the Prediction of the Force System in Face Milling Operation", *ASME Journal of Engineering for Industry*, Vol. 106(1), pp. 81-88.
- Gu, F., Melkote, S. N., Kapoor, S. G., and Devor, R. E., 1997, "A Model for the Prediction of Surface Flatness in Face Milling", *Journal of Manufacturing Science and Engineering Transaction of the ASME*, Vol. 119 (No. 4), pp. 476-484.
- Lazoglu, I., and Liang, S. Y., 1997, "Analytical Modeling of Force System in Ball End Milling", *Journal of Machining Science and Technology*, Vol. 1 (No.2), pp. 219-234
- Leu, M. C., Wang, L. and Blackmore, D., 1997, "A Verification Program for 5-axis NC Machining with General APT Tools", *Annals of the CIRP*, Vol. 46 (No. 1), pp. 419-424.
- Martellotti, M.E., 1945, "An Analysis of the Milling Process. Part II: Down Milling", *Transactions of the ASME*, Vol. 67, pp. 233-251.
- Montgomery, D. and Altintas, Y., 1991, "Mechanism of Cutting Force and Surface Generation in Dynamic Milling", *Transactions of ASME Journal of Engineering for Industry*, Vol. 113, pp. 160-168.
- Ramaraj, T. C. and Eleftheriou, E., 1994, "Analysis of the Mechanics of Machining with Tapered End Milling Cutters", *Transactions of the ASME*, Vol. 116, pp. 398-404.
- Spence, A., Altintas, Y., 1994, "A Solid Modeler Based Milling Process Simulation and Planning System", *Transactions of the ASME, Journal of Engineering for Industry*, Vol. 116, pp. 61-69.
- Spiewak S. A., 1994 "Analytical modeling of cutting point trajectories in milling", *Transactions of the ASME, Journal of Engineering for Industry*, Vol. 116 (No.4), pp. 440-448.
- Sutherland, J. W. and Devor, R. E., 1986, "An Improved Method for Cutting Force and Surface Error Prediction in Flexible end Milling System", *Transaction of ASME, Journal of Engineering for Industry*, Vol. 108, pp. 269-279.
- Yucesan, G. and Altintas, Y., 1996, "Prediction of Ball End Milling Forces", *Transaction of ASME, Journal of Engineering for Industry*, Vol. 1(No. 1), pp. 95-103.